

On the Hardware Feasibility of Nonlinear Trajectory Optimization for Legged Locomotion based on a Simplified Dynamics

Angelo Bratta^{1,2}, Romeo Orsolino², Michele Focchi², Victor Barasuol²,
Giovanni Gerardo Muscolo³ and Claudio Semini²

Abstract—We propose two feasibility constraints to be included in a Single Rigid Body Dynamics (SRBD)-based trajectory optimizer in order to obtain robust motions in challenging terrain. The former finds an approximate relationship between joint torque limits and admissible contact forces without requiring the joints' configuration. The latter proposes a model of the leg to guarantee the avoidance of the collision with the environment. Such constraints have been included in a nonlinear non-convex optimization problem. We validate the feasibility of the trajectories both in simulation and on the Hydraulically actuated Quadruped (HyQ) robot, including experiments with non flat terrain.

I. INTRODUCTION

Trajectory planning is a key element for the locomotion of legged robots. The more complex the terrain to be traversed, the harder it gets to find a set of joint commands that allows the robot to reach the desired target.

The literature on this topic is typically split between the usage of simplified dynamic models, such as the Linear Inverted Pendulum (LIP) [1] or the Spring Loaded Inverted Pendulum (SLIP) [2] and the usage of whole body models. The former are computationally efficient but only applicable to flat terrains; the latter guarantee more accurate description of the robot dynamics on arbitrary terrains but they require larger computational effort which is not suitable for real-time applications.

A third option is represented by the Centroidal Dynamics (CD) [3], [4] which exploits the full dynamics of a robot projected at its own Center of Mass (CoM). The CD is a precise description of robot's dynamics in terms of its inputs (feet and CoM wrenches) and outputs (feet and CoM trajectories); for this reason, it should therefore not be considered as an approximate dynamic model.

A simplification of the CD is the SRBD, where the robot is seen as a single rigid body with massless legs. Robot's inertia is fixed and corresponds to its aggregate inertia in a predefined configuration. This implies that, unlike the CD, the robot's CoM matches the CoM of the base and it therefore does not move with respect to the base frame.

Due to its simplicity, SRBD is well suited to problems which require computational efficiency while dealing with complex terrains and possible non-coplanar contacts. In

addition, it is a suitable approximation for robot with legs whose mass is negligible compared to the trunk's weight.

Since SRBD (as well as CD), however, only foresees the presence of the CoM and the robot's feet, it is possible that a motion planner based on this model finds a trajectory which violates feasibility constraints of the actual robot. Such constraints include the joint kinematic limits, the joint torque limits and the possible collisions between robot's links and the environment. A solution that violates these constraints is infeasible and can be dangerous for the robotic hardware unless carefully managed.

In this manuscript we address such limitations of the existing state-of-the-art nonlinear motion planners for legged robots based on SRBD, focusing, in particular, on the actuation consistency of the contact forces and on the legs' geometry to avoid shin collision.

A. Contributions

In this manuscript the following theoretical and experimental novelties are presented:

1) Theoretical contributions:

- a novel approximate, robot-agnostic, projection of the joint torque limits into the task space. To the best of our knowledge, this represents a novel approach to describe the existing relationship between the leg's configuration and the corresponding maximal contact forces at the end-effector. This allows motion planners based on nonlinear optimization to adjust the desired robot configuration and forces depending on the actuation capabilities of each leg, which is usually not captured by standard simplified models such as CD or SRBD;
- a novel model of the leg's lower link to include into the trajectory optimization formulation the finite non-zero size of the robot's feet and shin's geometry.

2) *Experimental contribution*: we present the hardware implementation of the trajectories obtained with a revisited version of the formulation presented by Winkler *et al.* [5] based on SRBD. The planner's trajectories have been tested on the HyQ [6] robot of Istituto Italiano di Tecnologia (IIT). This is the first time that trajectories based on [5] are deployed on a real hardware on non-flat terrains different from the flat, achievement which would not have been possible without the increased robustness guaranteed by the two feasibility constraints mentioned above.

¹ Department of Electronics and Telecommunications, Collegio di Ingegneria Informatica, del Cinema e Meccatronica, Politecnico di Torino, Turin (Italy).

²Dynamic Legged Systems (DLS) lab, Istituto Italiano di Tecnologia, Genova (Italy). email: angelo.bratta, romeo.orsolino, claudio.semini@iit.it.

³Department of Mechanical and Aerospace Engineering, Politecnico di Torino, Turin (Italy). email: giovanni.muscolo@polito.it

II. RELATED WORKS

The trade-off between simplicity of the model and feasibility of a whole-body motion on rough terrain is still at the core of the research in robotic legged locomotion. One approach consists in using the trajectory generated with CD (which is typically lower dimensional than the full dynamic model of the robot) in combination with the full robot kinematics to obtain a feasible whole-body motion [7], [8]. A similar approach was used by Valenzuela *et al.* [9] in which the authors compute the sequence of footholds using a Mixed Integer Convex optimization problem and then solve a nonlinear problem to find a linear and angular centroidal momentum trajectory. Budhiraja *et al.* [10] generated a trajectory for the CoM, in both the simplified and in the full dynamic model, making sure that the former is coherent with the latter. All these approaches have been only tested in simulation with a bipedal robot, but never on the robotic hardware.

Farshidian *et al.* [11] have introduced a nonlinear Model Predictive Control (MPC) which is able to compute the relevant motion quantities in a short amount of time suitable for interactive rates. The limit of this approach is that it requires a big computational effort and it can thus only plan few phases of the motion (*e.g.* one step prediction horizon).

Other authors leave on the motion controller the burden to verify the whole-body feasibility of the motion plan and focus, instead, on the nonlinearities which are present in the CD and SRBD formulations (mainly angular momentum and contact phases duration). These are usually tackled by either defining a convex relaxation of the formulation [12], [13], or by predefining the feet position for the entire trajectory [14].

Winkler *et al.* [5] implemented a trajectory optimization, based on the SRBD, in which CoM position, orientation, feet position, contact forces and their derivatives are concurrently optimized. The efficiency of this planner has been demonstrated both in simulation and on the real hardware on flat terrains. On rough terrains, however, only knowing the trajectory of the CoM and the feet is not enough to obtain a feasible whole body motion that can be deployed on the real robotic hardware as other feasibility constraints such as joint torque limits and geometry of the robot's legs need to be considered.

A state-of-art approach to the problem of avoiding collision between legs and ground is looking for a collision-free swing phase, considering the height map of the terrain and the robot configuration [15]. An alternative is presented in [16], in which the controller is able to detect the point of application of the ground reaction forces from the foot to the shin in case of collision. This method can guarantee safe navigation on challenging terrains, however, it is a pure reactive module which does not increase the robustness of the planner.

The joint torque limits constraint problem is usually only addressed at controller level [17], [18]. In order to explicitly consider this limit at the planning stage, Ding *et al.* [19] convexify the nonlinear joint torque constraint such that it

can be added to a Mixed Integer Quadratically Constrained Program (MIQCP). This formulation is suitable for convex optimization and it thus computationally efficient. The decision to employ a unique outer bounding ellipsoid as an approximation of the force ellipsoids, however, discards the important (configuration dependent) information regarding the relationship between the leg's configuration and shape of the force ellipsoids (*i.e.* the contact force is constant and it does not depend on the foot position).

Orsolino *et al.*, instead, used the force polytopes [20] to map the joint torques limits into a set of admissible centroidal wrenches [21] or CoM positions [22]. The former approach however, is not suitable for online foothold optimization because of its computational effort while the latter is only suitable for static gaits.

III. FORMULATION OF THE PROBLEM

We attempt to overcome the above limitations by defining a motion planner which solves a nonlinear, non-convex, trajectory optimization problem based on the SRBD and which includes some nonlinear constraints which will bias the solver towards a solution that is more coherent with the whole-body model of the specific robot.

A. Single Rigid Body Dynamics Model

The assumption of configuration independent CoM and inertia of the robot is a fair assumption especially for quadrupeds with legs of negligible mass compared to their trunk's mass, as in the case of HyQ [6]. The Newton-Euler equations lead to the following dynamic equation:

$$m\ddot{\mathbf{r}} = \sum_{i=1}^{n_i} \mathbf{f}_i(t) - m\mathbf{g} \quad (1)$$

$$\mathbf{I}\dot{\boldsymbol{\omega}}(t) + \boldsymbol{\omega}(t) \times \mathbf{I}\boldsymbol{\omega}(t) = \sum_{i=1}^{n_i} (\mathbf{f}_i(t) \times (\mathbf{r}(t) - \mathbf{p}_i(t))) \quad (2)$$

where m is the mass of the robot, $\mathbf{r} \in \mathbb{R}^3$ is the CoM position, $\ddot{\mathbf{r}} \in \mathbb{R}^3$ is the CoM linear acceleration, $\mathbf{f}_i \in \mathbb{R}^3$ are the contact forces, $n_i \in \mathbb{R}$ is the number of feet, $\mathbf{g} \in \mathbb{R}^3$ is the gravity vector, $\mathbf{I} \in \mathbb{R}^{3 \times 3}$ is the inertia matrix, $\boldsymbol{\omega} \in \mathbb{R}^3$ is the angular velocity, $\dot{\boldsymbol{\omega}} \in \mathbb{R}^3$ is the angular acceleration, and $\mathbf{p}_i \in \mathbb{R}^3$ is the cartesian position of foot i .

B. Kinematic Model

In order to guarantee that joint angles are inside their kinematic limits, the foot position with respect to the base is constrained to be inside a conservative approximation of the leg's workspace defined as a cube centered in the nominal foot position:

$$\mathbf{p}_i(t) \in \mathcal{R}_i \Leftrightarrow |\mathbf{p}_i(t) - \bar{\mathbf{p}}_i| < b \quad (3)$$

where $\bar{\mathbf{p}}_i \in \mathbb{R}^3$ is the nominal position for foot i and b is half of the length of the bounding box.

C. Terrain and Contact Models

Feet must be in contact with the terrain during the stance phase, while they have to be at positive height with respect to the terrain during the swing phase. This guarantees that there is no penetration into the terrain, but it is not sufficient to avoid shin collisions.

The contact model of [5] checks whether the contact force \mathbf{f}_i of every foot lies within the linearized friction cone \mathcal{F}_i . From a mathematical point of view it has to verify that:

$$\underline{d}_i < C_i \mathbf{f}_i < \bar{d}_i \quad (4)$$

$$C_i = \begin{bmatrix} (-\mu_i \mathbf{s}_i + \mathbf{t}_{1i})^T \\ (-\mu_i \mathbf{s}_i + \mathbf{t}_{2i})^T \\ (\mu_i \mathbf{s}_i + \mathbf{t}_{2i})^T \\ (\mu_i \mathbf{s}_i + \mathbf{t}_{1i})^T \\ \mathbf{s}_i^T \end{bmatrix} \quad \underline{d}_i = \begin{bmatrix} -\infty \\ -\infty \\ 0 \\ 0 \\ 0 \end{bmatrix} \quad \bar{d}_i = \begin{bmatrix} 0 \\ 0 \\ \infty \\ \infty \\ f_{max} \end{bmatrix} \quad (5)$$

where $\mathbf{s} \in \mathbb{R}^3$ is the normal direction to the terrain, μ is the friction coefficient, $\mathbf{f}_i \in \mathbb{R}^3$ is the contact force, \mathbf{t}_{1i} , \mathbf{t}_{2i} are the two tangential directions to the terrain and $i = 1, \dots, n_c$ where n_c is the number of feet in contact with the ground.

To sum up, the overall trajectory optimization program can be described as:

$$\begin{aligned} \text{find: } & \mathbf{x} = [\mathbf{r}^T, \boldsymbol{\theta}^T, \mathbf{p}_i^T, \mathbf{f}_i^T] \\ & \text{for } i = 0, \dots, n_c \\ \text{such that:} & \\ \text{(dynamic model)} & \quad [\ddot{\mathbf{r}}, \dot{\boldsymbol{\omega}}]^T = \mathbf{f}(\mathbf{r}, \boldsymbol{\theta}, \mathbf{p}_i, \mathbf{f}_i) \\ \text{(friction cone)} & \quad \mathbf{f}_i \in \mathcal{F}_i \\ \text{(foot position)} & \quad \mathbf{p}_i \in \mathcal{R}_i \\ \text{(force polytope)} & \quad \mathbf{f}_i \in \mathcal{A}_i \\ \text{(leg's geometry)} & \quad \mathbf{p}_i \in \mathcal{P}_i \end{aligned} \quad (6)$$

The above formulation corresponds to the one employed in Winkler *et al.* [5], except for the *force polytope* and the *leg's geometry* constraints that are the contribution of this work and are further explained in the following Section.

IV. GEOMETRY AND ACTUATION CONSISTENCY

In this Section, we propose a method to incorporate the joint torque limits constraint into the nonlinear optimization employed by our motion planner and another strategy to include the collision avoidance of foot and shin with the environment.

A. Joint Torques Limits

Traditional contact models neglect the existing relationship between the maximum contact force \mathbf{f}_i^{lim} and the limb configuration $\mathbf{q}_i \in \mathbb{R}^n$ (where n is the number of Degrees of Freedom (DoFs) of the leg). On the robotics hardware, admissible joint torques $\tau_i(\mathbf{q})$ are mapped into admissible contact forces \mathbf{f}_i at the i^{th} end-effector [20], [17], [21]. This mapping is represented by the leg's Jacobian $\mathbf{J}_i(\mathbf{q})$ matrix which is typically nonlinear and configuration dependent. From now, unless specified, all the quantities refer to one single leg and we can thus drop the pedex i :

$$\boldsymbol{\tau}^{lim} = \mathbf{J}(\mathbf{q})^T \mathbf{f}^{lim} \quad (7)$$

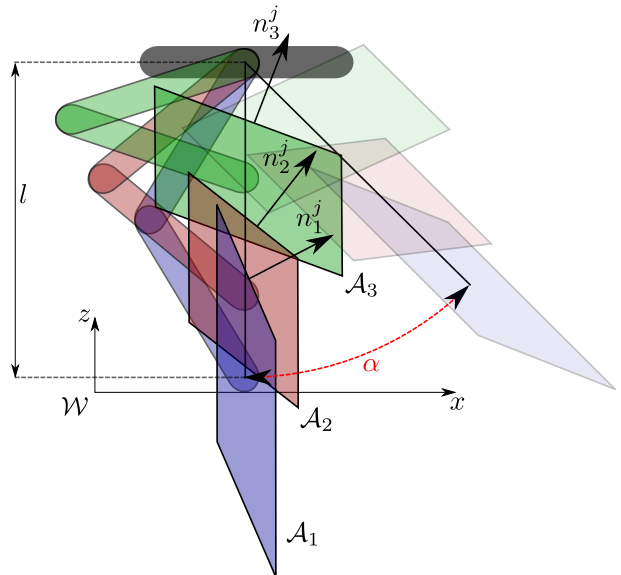


Fig. 1. Representation of a planar leg with 2 DoFs in three different configurations. For each configuration the corresponding force polytope is shown. The angle α represents the tilt angle of leg (*i.e.* angle between the vertical and the line connecting the foot and hip joint). l is instead the distance between foot and hip joint.

where \mathbf{f}^{lim} is one of the 2^n vertices of the leg's force polytope \mathcal{A} [23]. For a maximum joint torque value τ^{lim} , the polytope \mathcal{A} can be employed to relate the feet's position and velocity to the maximum contact forces that the robot can perform on the ground. This is an important feature that needs to be considered whenever the robot needs to take on complex configurations in order to negotiate rough terrains such as steps and non-coplanar contacts. In Fig. 1 we can see a planar example where three force polytopes \mathcal{A}_k (with $k = 1 \dots 3$) are computed for the three different configurations of the same planar leg. In this example, we decided to pick three polytopes because it allows us to sample the force polytopes at the configuration of maximum retraction, of maximum extension and at the leg's nominal configuration. In all the three cases the end-effector is located on the same line at a distance of l_k from the leg's hip joint. The variable l represents the distance between the foot and the hip joint:

$$l = \sqrt{(p_x^b - h_x^b)^2 + (p_z^b - h_z^b)^2} \quad (8)$$

The considered leg has 2 DoFs and, therefore, all the force/wrench polytopes are made of $2n = 4$ halfspaces. Each halfspace can be represented by its normal unit vector $\mathbf{n}_k^j \in \mathbb{R}^m$ (with $j = 1 \dots 2n$) and the known term $d_k^j \in \mathbb{R}$. For instance, the generic force polytope \mathcal{A}_k can be expressed as:

$$\mathcal{A}_k = \left\{ \mathbf{f} \in \mathbb{R}^m \mid \mathbf{A}_k(\mathbf{q})\mathbf{f} \leq \mathbf{d}_k(\mathbf{q}) \right\} \quad (9)$$

where m is the dimension of the contact force (*e.g.* $m = 2$ in the planar case of Fig. 1 with a point foot) and:

$$\mathbf{A}_k(\mathbf{q}) = [\mathbf{n}_k^1, \dots, \mathbf{n}_k^{2n}]^T \quad (10)$$

The rows of the $\mathbf{A}_k(\mathbf{q})$ matrix are related to the rows of the leg's transposed Jacobian $\mathbf{J}(\mathbf{q})^T$. As we are interested in the way the matrix $\mathbf{A}_k(\mathbf{q})$ changes with respect to a variation of the foot \mathbf{p} in the cartesian space, we should then analyze the quantity $d\mathbf{J}(\mathbf{q})/d\mathbf{p}$. This is, however, robot-specific and goes against the assumption of SRBD. For this reason, we then propose an approximate approach that is robot-agnostic. It therefore keeps the relationship between foot position and maximal contact forces without the need of explicitly knowing the morphology of the considered robot.

For that purpose, we assume that the transformation between the corresponding halfplanes of two polytopes \mathcal{A}_a and \mathcal{A}_b consists of an homogeneous transformation instead of considering the actual dependency from the robot's configuration manifold \mathbf{q} . In particular, the homogeneous transformation is composed of a rotation of the leg's tilt angle α and a linear interpolation performed on the term d^j . More in depth, α corresponds to the angle between the vertical and the line that connects the foot to the hip joint (see Fig. 1):

$$\alpha = \arctan\left(\frac{p_x^b - h_x^b}{p_z^b - h_z^b}\right) \quad (11)$$

where (h_x^b, h_z^b) is the fixed position of the hip joint and (p_x^b, p_z^b) is the foot position with respect to the base frame. $\mathbf{R}(\alpha) \in \mathbb{R}^{2 \times 2}$ rotates the obtained force polytope by the angle α in such a way to align it to the leg. We can therefore consider l and α as the polar coordinates of the foot with respect to the hip joint.

The generic normal unit vector $\mathbf{n}^j(l)$ is found as the geodesic average [24] of the two neighboring values l_a and l_b :

$$\mathbf{n}^j = \mathbf{R}(\alpha) \begin{bmatrix} \cos(\theta) \\ \sin(\theta) \end{bmatrix} \quad (12)$$

where:

$$\theta = \frac{l - l_a}{l_b - l_a}(\theta_b - \theta_a) + \theta_a \quad (13)$$

θ_a and θ_b are the angles corresponding to the two *predefined* normal vectors $\mathbf{n}_a = [\cos(\theta_a), \sin(\theta_a)]^T$ and $\mathbf{n}_b = [\cos(\theta_b), \sin(\theta_b)]^T$ closest to the value of l (see Fig. 2).

The generic known term d can be found as a linear interpolation between the values d_a and d_b :

$$d = \frac{l - l_a}{l_b - l_a}(d_b - d_a) + d_a \quad (14)$$

The variables $(\cdot)_a$ and $(\cdot)_b$ take on the values corresponding to the two neighboring force polytopes \mathcal{A}_a and \mathcal{A}_b :

$$\begin{cases} (\cdot)_a = (\cdot)_1^j, & (\cdot)_b = (\cdot)_2^j & \text{if } l_1 \leq l \leq l_2 \\ (\cdot)_a = (\cdot)_2^j, & (\cdot)_b = (\cdot)_3^j & \text{if } l_2 < l \leq l_3 \end{cases} \quad (15)$$

Equations (12), (13) and (14) represent a polytope morphing among the three reference polytopes computed at the three predefined configurations. Despite the nonlinearity given by the trigonometric terms in (12), this morphing represents a significant simplification because it does not require the knowledge of the leg's Jacobian matrix at the considered leg configuration. This morphing is well suited

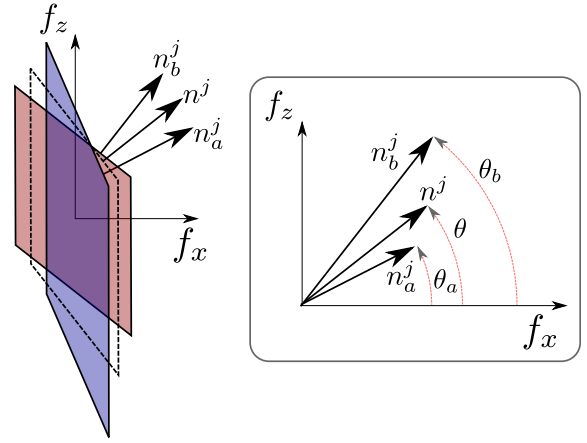


Fig. 2. Geodesic average of the unit vectors \mathbf{n}_a and \mathbf{n}_b normal to the halfplanes of the force polytopes \mathcal{A}_a and \mathcal{A}_b . The generic normal vector \mathbf{n}^j is obtained by linear interpolation of the angles θ_a and θ_b .

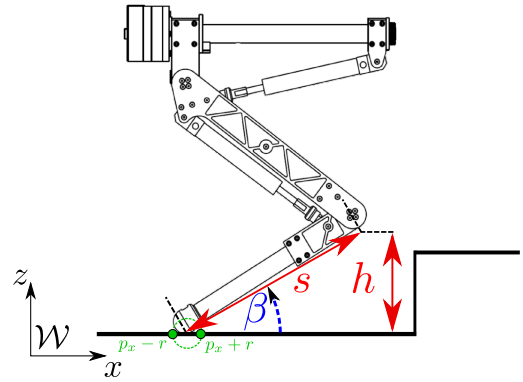


Fig. 3. Representation of one single leg of the HyQ robot. h is the knee height, s is the length of the lower link and β is the angle selected to keep the shin from hitting possible obstacles. r is the radius of the foot used to avoid edges and unsafe foothold.

for trajectory optimization formulations such as the one described in (6) where the optimization variables \mathbf{x} only include operational space quantities such as \mathbf{r} and \mathbf{p} .

B. Environment Collision Avoidance

As introduced in Section I, the SRBD considers point feet, while in the real robots feet always have a non-negligible size. In this Section, we include the radius of HyQ's spherical feet in the formulation in such a way to discard solutions that may lead to undesired collisions during swing phase or to unsafe footholds in relation obstacles and rough terrains. Unsafe footholds, for example, happen when the spherical foot does not step entirely on the terrain (*e.g.* edge of a step). To overcome this, we force the planner to find a foothold \mathbf{p} in which the terrain height is constant at a radius r before and behind the considered foothold along the robot's direction of motion (see Fig. 3). The value of r is 2cm in the case of the HyQ robot. Moreover, the leg's volume plays an important role in the execution of successful motion plans, as it may lead to self-collisions or to collisions with the environment if not properly managed. Shin collisions, for example, may occur during a leg's stance phase as a consequence of a

wrong choice of the foothold or it may occur during the leg's swing phase. In order to avoid such collisions, we provide a simplified kinematic model of the leg to the motion planner. We assume the lower link to be a straight line of length s (distance between the foot's contact point and the knee) with a fixed angle β with respect to the ground. The knee's projection on the ground is equal to $s \cos(\beta)$ and the height of the knee corresponds to $h = s \sin(\beta)$ and it can then be mapped along the direction of motion using the knowledge of the yaw angle γ . Knee collision can thus be avoided if the height of the knee is higher than the terrain on that point. Fig. 3 represents the model chosen for the i^{th} leg in the x - z plane:

$$\begin{aligned} p_z + s \cdot \sin(\beta) &> h_{terrain}(p_{knee}) \\ p_{knee_x} &= p_x + s \cos(\beta) \cos(\gamma) \\ p_{knee_y} &= p_y + s \cos(\beta) \sin(\gamma) \end{aligned} \quad (16)$$

where $h_{terrain}(p_{knee}) \in \mathbb{R}$ is the height of the terrain in the 2D projection of the knee, computed through (16).

Besides checking for possible knee collisions, we also avoid shin collisions by imposing the constraint on a number of points between the foot and the knee. The lower limb length s is a constant robot parameter while a conservative value of β angle should be selected by looking at the maximum inclination that the leg assumes during a walk.

V. SIMULATION AND EXPERIMENTAL RESULTS

In this Section we present the validation results that have lead to the successful execution of the optimal trajectories generated by our motion planner on the HyQ robot both in simulation and on the real hardware. For all the simulations and experiments we used an Intel Core i5-4460 CPU @ 3.20GHz \times 4 and all the nonlinear optimization problems were solved using an Interior Point method [25] solver, implemented in the IPOPT library [26].

A. Joint Torque Limits Approximation

Fig. 5 shows the Hip Abduction-Adduction (HAA), Hip Flexion-Extension (HFE) and Knee Flexion-Extension (KFE) joint torques and the corresponding saturation limits of the HyQ robot during a 1m walk on a flat terrain for 2.4s (three crawl gait cycles).

The plots show the optimal trajectory obtained using the motion planner with (right) and without (left) the force polytope constraints. Our motion planner does not explicitly optimize over joint torques τ , however it is possible to compute the τ exploiting the dynamic equation of motion of each single leg:

$$\tau = \mathbf{M}\ddot{\mathbf{q}} + \mathbf{c}(\mathbf{q}, \dot{\mathbf{q}}) + \mathbf{g}(\mathbf{q}) - \mathbf{J}(\mathbf{q})^T \mathbf{f} \quad (17)$$

\mathbf{f} is the contact force as optimized by the motion planner and $\mathbf{q}, \dot{\mathbf{q}}, \ddot{\mathbf{q}}$ can be obtained by inverse kinematics of the foot trajectory in the base frame \mathbf{p}^b (assuming a fixed offset between base and robot's CoM). \mathbf{M}, \mathbf{c} and \mathbf{g} represent, respectively, the leg's inertial matrix, the Coriolis and the gravity term. We can see in the left plots that the desired torques violate the saturation limits of the actuators of the HyQ robot. This is



Fig. 4. HyQ robot stepping up a pallet of 10cm in both simulation (Gazebo) and hardware experiment.

justifiable considering that the baseline motion planner has no information about such saturation values and the only constraints acting on the contact forces are the linearized friction cones. The plots on the right, instead, do not violate

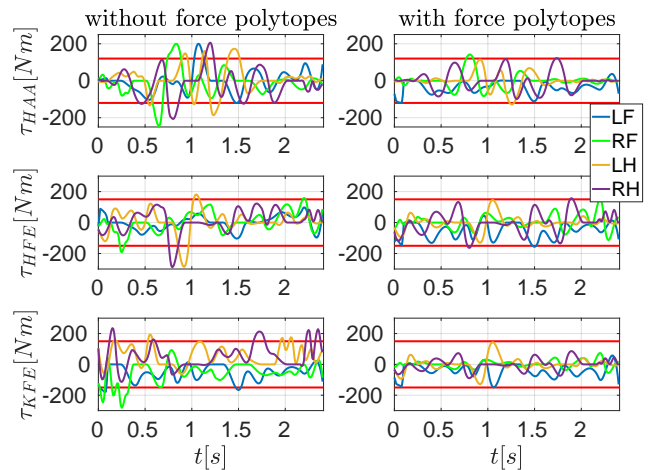


Fig. 5. This plot shows the joint torques of the HyQ robot over a 2.4m walk on a flat terrain. We can see, in the case where no force polytopes are considered (left plots), that the torques τ_{HAA}, τ_{HFE} and τ_{KFE} violate their limits multiple times during the walk. On the right plots, instead, we can see that the force polytope constraint is able to bias the planner towards a solution that respects all the limits.

the torque limits of the robot thanks to the force polytope constraint included in the motion planner formulation. This is possible thanks to more extended configuration that the HyQ takes on during the walk and the standing phases. As a matter of fact, a force polytope with a larger maximum normal force corresponds to this robot configuration (see Fig. 1) [22].

Fig. 6 shows similar results for the monopod robot (corresponding to a single leg of HyQ, see Fig. 3).

B. Shin Collision Avoidance

Exploiting the constraint that we described in Section IV-B, HyQ was able to walk for 1m, performing three cycles of crawl in 11s to step onto 15cm high pallet in simulation and onto 10cm high pallet on the hardware robot. Fig. 7 shows the base position x (continuous line) and tracking error (dashed line) with respect to the desired trajectory computed by the planner in three following different versions:

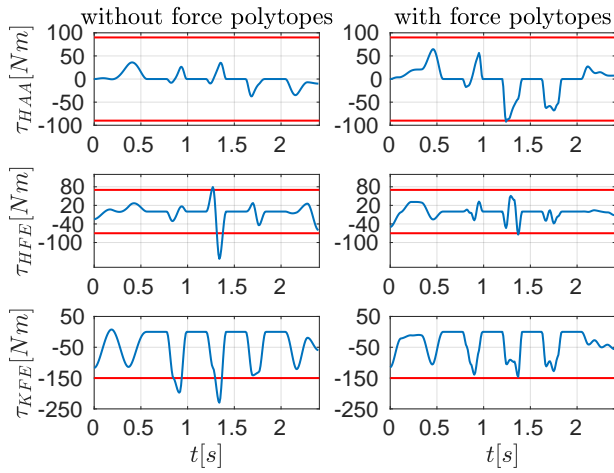


Fig. 6. This plot shows the joint torques of the monopod robot over a 2.4s motion on a flat terrain. We can see, in the case where no force polytopes are considered (left plots), that the HFE torque τ_{HFE} limit is violated twice during the hop (at $t = 0.9s$ and at $t = 1.3s$). On the right plots, instead, we can see that the force polytope constraint is able to bias the planner towards a solution that respects all the limits.

1) *Zero Size Point Foot and No Shin Collision Avoidance (red lines)*: This corresponds to the formulation given in [5] in which both shin collision and the foot size are neglected. The algorithm took $\sim 50s$ to find an optimal solution. In the upper plot of Fig. 7 we can see that, in this case, the tracking error (dashed line) grows until the experiment is stopped because the robot falls down. As it can be seen in the attached video¹ the robot collides with the corner of the edge, due to a non-robust choice of the foothold. The attached video shows that even a terrain with a relatively low obstacle (10cm) cannot be overcome without explicitly considering the feet and leg geometry.

2) *Non-Zero Size Point Foot and No Shin Collision Avoidance (green lines)*: In this case we enforce in the planner a foot radius r of 2cm, while we do not include any shin collision avoidance constraint. The computation time increased by 30 % compared to the first scenario ($\sim 70s$) in the case of 10cm high pallet. For the 15cm high pallet the solver took 105s to find an optimal solution. This constraint guarantees the successful navigation in the non flat terrain, but comparing the upper and the middle plot of Fig. 7 it can be seen that increasing of the height of the step will also increase the tracking error.

3) *Non-Zero Size Point Foot and Shin Collision Avoidance (blue lines)*: This version corresponds to the constraint described in Section IV-B. In case of a 10cm high pallet, the algorithm took twice as long as the first simulation ($\sim 100s$), while 130s were required in case of a 15cm high pallet. As robot parameter, the lower link length on HyQ s is 0.3m. Due to the symmetric design of HyQ, we have selected inclination angle $\beta=37^\circ$ for the hind legs and $\beta=127^\circ$ for the front legs. The shin collision is thus possible on HyQ only with hind legs when walking up a step and front legs when walking down a step; which is automatically captured

¹https://youtu.be/rGrQ_9YwQxw

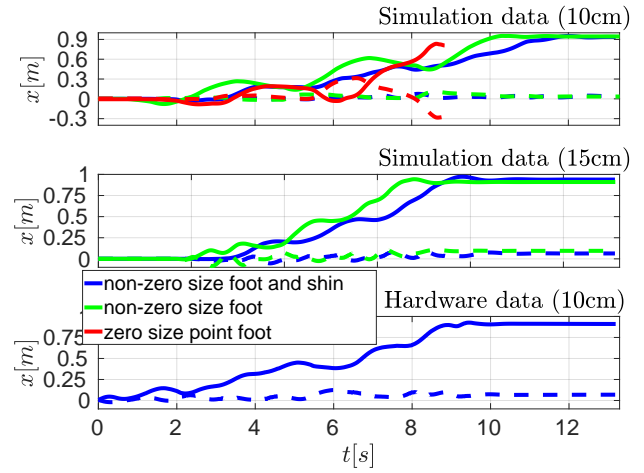


Fig. 7. Shin collision planning: tracking performances of simulations with three different terrain constraints for a walk of 1m with three crawl cycles. The thick lines represent the base position x while the dashed lines represent the tracking error with respect to the desired trajectory along the same x coordinate.

by the definition of the constraint defined in (16). For this experiment we selected two points, besides the knee, to be checked against possible collisions. Unlike the previous version of the planner, in this case the tracking error did not increase in the case of higher step thanks to the larger robustness given by the shin collision avoidance constraint. In the attached video, we can see the robot stepping onto a 10cm pallet which is, to the best of our knowledge, the first hardware implementation of a trajectory planner based on [5] on a non-flat terrain.

VI. CONCLUSION

In this paper we presented two theoretical contributions consisting of two feasibility constraints aimed at increasing the robustness of trajectories that are optimized using the SRBD model. The first constraint focuses on including the joint torque limits constraint and approximates the way these limits are mapped into admissible contact forces depending on the leg's configuration. The proposed approximation is robot-independent and is thus suitable for motion planning applications based on simplified robot-agnostic models, such as SRBD or CD. The second constraint, instead, is able to describe and approximate the volume of the robot's legs in such a way to avoid undesired collisions between the lower limbs and the environment.

The experimental contribution of this paper consists of the hardware deployment of the optimal trajectories obtained with the formulation of [5] which would not have been possible on non-flat terrain without the feasibility constraints that we proposed above.

Future works include the development of strategies for online replanning (the solver optimizes while the robot walks) and the usage of pre-computed feasible solutions for the warm start of every new nonlinear trajectory optimization. The successful roll-out of planned trajectories relies on a precise identification of the robot's inertial parameters

(robot's CoM and inertia tensors) which is also object of our future works.

REFERENCES

- [1] S. Kajita, F. Kanehiro, K. Kaneko, K. Yokoi, and H. Hirukawa, "The 3d linear inverted pendulum mode: a simple modeling for a biped walking pattern generation," in *IEEE/RSJ International Conference on Intelligent Robots and Systems*, vol. 1, Oct 2001, pp. 239–246 vol.1.
- [2] H. Geyer and U. Saranli, *Gait Based on the Spring-Loaded Inverted Pendulum*. Dordrecht: Springer Netherlands, 2018, pp. 1–25.
- [3] D. E. Orin, A. Goswami, and S.-H. Lee, "Centroidal Dynamics of a Humanoid Robot," *Auton. Robots*, vol. 35, no. 2-3, pp. 161–176, 2013. [Online]. Available: <http://dx.doi.org/10.1007/s10514-013-9341-4>
- [4] P. M. Wensing and D. E. Orin, "Improved Computation of the Humanoid Centroidal Dynamics and Application for Whole-Body Control," *International Journal of Humanoid Robotics*, vol. 13, no. 1, 2016.
- [5] A. W. Winkler, C. D. Bellicoso, M. Hutter, and J. Buchli, "Gait and Trajectory Optimization for Legged Systems through Phase-based End-Effector Parameterization," *IEEE Robotics and Automation Letters (RA-L)*, pp. 1560–1567, 2018. [Online]. Available: <http://ieeexplore.ieee.org/document/8283570/>
- [6] C. Semini, N. G. Tsarakakis, E. Guglielmino, M. Focchi, F. Cannella, and D. G. Caldwell, "Design of HyQ -A hydraulically and electrically actuated quadruped robot," *Proceedings of the Institution of Mechanical Engineers. Part I: Journal of Systems and Control Engineering*, vol. 225, no. 6, pp. 831–849, 2011.
- [7] H. Dai, "Whole-body motion planning with centroidal dynamics and full kinematics," *IEEE-RAS International Conference on Humanoid Robots*, 2014.
- [8] A. Herzog, S. Schaal, and L. Righetti, "Structured contact force optimization for kino-dynamic motion generation," in *2016 IEEE/RSJ International Conference on Intelligent Robots and Systems (IROS)*, Oct 2016, pp. 2703–2710.
- [9] A. K. Valenzuela, "Mixed-integer convex optimization for planning aggressive motions of legged robots over rough terrain," 2016. [Online]. Available: <https://dspace.mit.edu/handle/1721.1/103432>
- [10] R. Budhiraja, J. Carpentier, and N. Mansard, "Dynamics Consensus between Centroidal and Whole-Body Models for Locomotion of Legged Robots," *ICRA 2019 - IEEE International Conference on Robotics and Automation*, 2019. [Online]. Available: <https://hal.laas.fr/hal-01875031>
- [11] F. Farshidian, E. Jelavic, A. Satapathy, M. Gifftthaler, and J. Buchli, "Real-Time motion planning of legged robots: A model predictive control approach," *IEEE-RAS International Conference on Humanoid Robots*, pp. 577–584, 2017.
- [12] H. Dai and R. Tedrake, "Planning robust walking motion on uneven terrain via convex optimization," *IEEE-RAS International Conference on Humanoid Robots (Humanoids)*, 2016.
- [13] B. Ponton, A. Herzog, A. Del Prete, S. Schaal, and L. Righetti, "On time optimization of centroidal momentum dynamics," 2018. [Online]. Available: <https://arxiv.org/pdf/1810.13082.pdf>
- [14] J. Di Carlo, P. M. Wensing, B. Katz, G. Bleth, and S. Kim, "Dynamic Locomotion in the MIT Cheetah 3 Through Convex Model-Predictive Control," *IEEE International Conference on Intelligent Robots and Systems*, no. January 2019, pp. 7440–7447, 2018.
- [15] F. Doshi, E. Brunskill, A. Shkolnik, T. Kollar, K. Rohanimanesh, R. Tedrake, and N. Roy, "Collision detection in legged locomotion using supervised learning," *IEEE International Conference on Intelligent Robots and Systems*, pp. 317–322, 2007.
- [16] V. Barasuol, G. Fink, M. Focchi, D. Caldwell, and C. Semini, "On the Detection and Localization of Shin Collisions and Reactive Actions in Quadruped Robots," *22nd International Conference on Climbing and Walking Robots*, 2019.
- [17] V. Samy, S. Caron, K. Bouyarmane, and A. Kheddar, "Post-Impact Adaptive Compliance for Humanoid Falls Using Predictive Control of a Reduced Model."
- [18] S. Fahmi, C. Mastalli, M. Focchi, and C. Semini, "Passivity Based Whole-body Control for Quadrupedal Locomotion on Challenging Terrain," *ArXiv*, 2018.
- [19] Y. Ding, C. Li, and H. W. Park, "Single Leg Dynamic Motion Planning with Mixed-Integer Convex Optimization," *IEEE International Conference on Intelligent Robots and Systems*, pp. 7391–7396, 2018.
- [20] P. Chiacchio, Y. Bouffard-Vercelli, and F. Pierrot, "Force Polytope and Force Ellipsoid for Redundant Manipulators," *Journal of Robotic Systems*, vol. 14, no. 8, pp. 613–620, 1997.
- [21] R. Orsolino, M. Focchi, C. Mastalli, H. Dai, D. G. Caldwell, and C. Semini, "Application of Wrench based Feasibility Analysis to the Online Trajectory Optimization of Legged Robots," *IEEE Robotics and Automation Letters (RA-L)*, pp. 3363–3370, 2018.
- [22] R. Orsolino, M. Focchi, S. Caron, G. Raiola, V. Barasuol, and C. Semini, "Feasible Region: an Actuation-Aware Extension of the Support Region," 2019. [Online]. Available: <https://arxiv.org/abs/1903.07999>
- [23] B. Siciliano and O. Khatib, *Springer Handbook of Robotics*. Berlin, Heidelberg: Springer-Verlag, 2007.
- [24] C. Gramkow, "On averaging rotations," *Journal of Mathematical Imaging and Vision*, vol. 15, no. 1, pp. 7–16, Jul 2001. [Online]. Available: <https://doi.org/10.1023/A:1011217513455>
- [25] H. Yamashita, "A global convergent primal-dual interior point method for constrained optimization," *Optimization Methods and Software*, vol. 10, pp. 443–469, 1998.
- [26] A. Wächter and L. T. Biegler, "On the implementation of an interior-point filter line-search algorithm for large-scale nonlinear programming," *Mathematical Programming*, vol. 106, no. 1, pp. 25–57, mar 2006. [Online]. Available: <https://doi.org/10.1007/s10107-004-0559-y>